Computational and Structural Biotechnology Journal 19 (2021) 145–152

COMPUTATIONAL AND STRUCTURAL BIOTECHNOLOGY JOURNAL

journal homepage: www.elsevier.com/locate/csbj

Crystal structure of AmpC BER and molecular docking lead to the discovery of broad inhibition activities of halisulfates against β-lactamases

Bo-Gyeong Jeong [a], Jung-Hyun Na [a,1], Da-Woon Bae [a], Soo-Bong Park [a], Hyi-Seung Lee [b,*], Sun-Shin Cha [a,*]

[a] Department of Chemistry & Nanoscience, Ewha Womans University, Seoul 03760, Republic of Korea
[b] Marine Natural Products Chemistry Laboratory, Korea Institute of Ocean Science and Technology, Busan 49111, Republic of Korea

ARTICLE INFO

Article history:
Received 10 October 2020
Received in revised form 8 December 2020
Accepted 13 December 2020
Available online 17 December 2020

Keywords:
Crystal structure
AmpC BER
R2 loop
Marine natural products
Halisulfates
Broad-spectrum competitive inhibitors

ABSTRACT

AmpC BER is an extended-spectrum (ES) class C β-lactamase with a two-amino-acid insertion in the *H*10 helix region located at the boundary of the active site compared with its narrow spectrum progenitor. The crystal structure of the wild-type AmpC BER revealed that the insertion widens the active site by restructuring the flexible *H*10 helix region, which is the structural basis for its ES activity. Besides, two sulfates originated from the crystallization solution were observed in the active site. The presence of sulfate-binding subsites, together with the recognition of ring-structured chemical scaffolds by AmpC BER, led us to perform *in silico* molecular docking experiments with halisulfates, natural products isolated from marine sponge. Inspired by the snug fit of halisulfates within the active site, we demonstrated that halisulfate 3 and 5 significantly inhibit ES class C β-lactamases. Especially, halisulfate 5 is comparable to avibactam in terms of inhibition efficiency; it inhibits the nitrocefin-hydrolyzing activity of AmpC BER with a K_i value of 5.87 μM in a competitive manner. Furthermore, halisulfate 5 displayed moderate and weak inhibition activities against class A and class B/D enzymes, respectively. The treatment of β-lactamase inhibitors (BLIs) in combination with β-lactam antibiotics is a working strategy to cope with infections by pathogens producing ES β-lactamases. Considering the emergence and dissemination of enzymes insensitive to clinically-used BLIs, the broad inhibition spectrum and structural difference of halisulfates would be used to develop novel BLIs that can escape the bacterial resistance mechanism mediated by β-lactamases.

1. Introduction

β-Lactam antibiotics are suicide inhibitors against penicillin-binding proteins (PBPs) that are essential to synthesize the mesh-like peptidoglycan layer. Thanks to their low toxicity and their effectiveness in various bacteria, β-lactam antibiotics are the most widely prescribed chemotherapeutic agents to treat bacterial infections. However, their clinical usage has been promoting the emergence and spread of pathogens that are not eradicated by antibiotic treatment. The prevalent resistant mechanism of those bacteria is the production of β-lactamases [1]. β-Lactam antibiotics are structurally featured by a common β-lactam ring and β-lactamases inactivate them by hydrolytically break the reactive amide bond in the ring. Class A, C, and D β-lactamases have an active site serine residue for the nucleophilic attack on the ring amide bond while class B metallo-β-lactamases exploit a water molecule activated by zinc to cleave the ring.

To circumvent the β-lactamase-mediated antibiotic resistance threat, β-lactamase inhibitors (BLIs) have been developed [2]. A combination of β-lactam antibiotics and BLIs is a working strategy to treat β-lactamase-producing pathogens. Among BLIs, clavulanate, tazobactam, sulbactam, avibactam, and vaborbactam are

Abbreviations: ES, extended-spectrum; BLI, β-lactamase inhibitor; PBP, penicillin-binding protein; DBO, diazabicyclooctane; Ni-NTA, nickel-nitrilotriacetic acid; MES, 2-(N-morpholino) ethanesulfonic acid.

* Corresponding authors at: Protein Research Laboratory, Department of Chemistry & Nanoscience, Ewha Womans University, Seoul, 03760, Republic of Korea (S.-S. Cha), Marine Natural Products Chemistry Laboratory, Korea Institute of Ocean Science and Technology, 385 Haeyang-ro, Yeongdo-gu, Busan 49111, Republic of Korea (H.-S. Lee).

E-mail addresses: hslee@kiost.ac.kr (H.-S. Lee), chajung@ewha.ac.kr (S.-S. Cha).

[1] Present Address: Department of Pharmaceutical Engineering, Sangji University, Wonju 26339, Republic of Korea.

https://doi.org/10.1016/j.csbj.2020.12.015

widely used in therapy. However, clavulanate, tazobactam, sulbactam are only effective towards class A enzymes [3], and even the recently-developed avibactam and vaborbactam have a limited effect on class D β-lactamases and no effect on class B β-lactamases [4,5]. Furthermore, variants of class A β-lactamases which are not inhibited by avibactam have also been reported [6]. Notably, clinically applicable BLIs are similar to β-lactam antibiotics in terms of structure; they have a β-lactam ring or β-lactam-mimicking ring structure such as diazabicyclooctane (DBO) and cyclic boronic acid pharmacophore. Consequently, existing BLIs have limits in their structures and inhibition spectra, which would be overcome by the development of novel BLIs with a different structural scaffold.

AmpC BER is an extended-spectrum (ES) class C β-lactamase isolated from an *Escherichia coli* clinical strain and it has improved catalytic efficiencies (k_{cat}/K_m) for cephalosporins and imipenem than its progenitor AmpC EC2 [7]. ES class C enzymes are generally characterized by high k_{cat} and K_m values against diverse substrates compared to their progenitors. Despite the simultaneous increase of k_{cat} and K_m [8–10], the catalytic efficiency (k_{cat}/K_m) of ES class C β-lactamases can be elevated since the increase in k_{cat} is more than compensative for the increased K_m. In the case of AmpC BER, however, the k_{cat} increase is accompanied by the K_m decrease [8–10], which is ideal to increase the k_{cat}/K_m value, that is, to enhance the catalytic efficiency.

The only sequence difference between AmpC BER and AmpC EC2 is the existence of two more residues in the *H*10 helix region (residues 293–296) defining the boundary of the active site. Thus, the insertion mutation that affects the active site conformation is probably responsible for the unusual catalytic feature of AmpC BER. To reveal the structural consequence of the insertion mutation, we have determined the 1.79 Å resolution crystal structure of the wild-type AmpC BER. Although the *H*10 helix region was reported to be disordered in the previous study about the Ser64Ala mutant of AmpC BER [11], the wild-type structure has the ordered *H*10 helix region that allows depicting the conformational change of the active site induced by the insertion mutation. In addition, two sulfate-binding subsites are identified in the active site, which, together with the ability of AmpC BER to recognize the ring-structured scaffold, led us to demonstrate the inhibition activities of halisulfates isolated from marine sponges against β-lactamases. Their distinct chemical scaffold could be exploited to develop novel inhibitors that can escape bacterial resistant mechanisms adapted to existing BLIs.

2. Materials and methods

2.1. Cloning, expression, and purification of β-lactamases

Cloning of KPC-2, NDM-1, CMY-10, AmpC BER, and OXA-10 was performed as described previously [12]. The *E. coli* strain BL21 (DE3) was used as a host for heterologous expression of β-lactamases. At OD_{600} = ~0.5, their expression was induced by adding isopropyl β-D-1-thiogalactopyranoside at a final concentration of 1 mM. The induced cells were cultivated at 20 °C for 18 h and harvested by centrifugation. The cell pellets were resuspended in a 50 mM Tris-HCl (pH 7.4) buffer, and disrupted by sonication. The crude lysate was centrifuged and the resulting supernatant was loaded onto a nickel-nitrilotriacetic acid (Ni-NTA) column (GE Healthcare, USA). Then, eluted proteins from the Ni-NTA column were further purified by successively using a Superdex 75 HR 16/60 columns (GE Healthcare, USA) and *m*-aminophenylboronic acid agarose (Sigma-Aldrich, USA).

2.2. Crystallization and structure determination

AmpC BER in a buffer of 20 mM Tris-HCl pH 7.0 was concentrated to ~ 30 mg/ml and crystallized under the microbatch crystallization set up modified by our group [13,14]. Crystals belonging to the space group $P2_12_12_1$ (a = 60.855 Å, b = 64.484 Å, and c = 176.300 Å) were grown at 22 °C in drops under a thin layer of Al's oil that consist of 1 μl protein sample and an equal volume of a precipitant solution (0.2 M lithium sulfate, 0.1 M bis-tris pH 5.5, and 25% polyethylene glycol 3,350). To collect diffraction data, crystals were flash-cooled after a one-minute soak in a buffer composed of 0.2 M lithium sulfate, 0.1 M bis-tris pH 6.5, and 25% polyethylene glycol 3,350. A 1.79 Å resolution data set was processed and scaled using the *HKL*-2000 program suite [15]. Two promising positions of AmpC BER in the asymmetric unit were obtained by the molecular replacement program *MOLREP* [16] with the structure of AmpC EC2 (PDB code 5GGW) as a search model. The subsequent model building and refinement processes with *Coot* [17] and *PHENIX* [18] gave rise to a final model with the final *R* and R_{free} values of 17.1% and 21.2%, respectively (Table S1).

2.3. Extraction and isolation of halisulfates

Extraction of halisulfates 1, 3, and 5 were performed as described previously [19,20]. Freshly collected specimens of *Coscinoderma* sp. (voucher collection-number 122CH-837) were immediately frozen and stored at – 25 °C until use. Lyophilized specimens (432 g) were repeatedly extracted with MeOH (2 L × 2) and CH_2Cl_2 (2 L × 1). The combined extracts (37.9 g) were successively partitioned between H_2O (12.8 g) and *n*-BuOH (25.2 g); the organic fraction was repartitioned between MeOH-H_2O (85:15) (18.7 g) and *n*-hexane (6.4 g). An aliquot of the former layer (4.93 g) was separated by C_{18} reversed-phase vacuum flash chromatography with a stepwise gradient solvent system [MeOH-H_2O (5:5), (6:4), (7:3), (8:2), (9:1), (10:0), and EtOAc] to yield seven fractions. Based on the results of ^{1}H NMR, the fractions eluted with MeOH-H_2O (8:2) (1.35 g) and MeOH-H_2O (9:1) (0.76 g) were chosen for separation. The fraction eluted with MeOH-H_2O (8:2) was separated by semipreparative reversed-phase HPLC (YMC-ODS column, 10 mm × 250 mm; MeOH-H_2O, 6:4), yielding halisulfate 1. The eluted fraction with MeOH-H_2O (9:1) was separated by reversed-phase HPLC (YMC-ODS column, 10 mm × 250 mm; MeCN-H_2O, 4:6) to yield halisulfate 3, halisulfate 5. The purified metabolites (>95% purity) were isolated in the following amounts: 954.4 mg (halisulfate 1), 32.5 mg (halisulfate 3), and 61.1 mg (halisulfate 5). The molecular weight and purity of halisulfates were estimated on the basis of combined spectroscopic analyses and comparison of spectroscopic data including ^{1}H NMR and mass spectrometry with those in the literature [19,20] (Fig. S1 and S2).

2.4. Inhibition assays

To evaluate the relative inhibition efficacy of halisulfates toward different β-lactamases in a 50 mM MES [2-(N-morpholino) ethanesulfonic acid] (pH 6.5) buffer containing 4% dimethyl sulfoxide, enzyme concentration was fixed at 200 pM with different halisulfates concentrations (200 μM for KPC-2/CMY-10/AmpC BER/OXA-10, and 1 mM for NDM-1). After the addition of 100 μM nitrocefin, the absorbance of the nitrocefin hydrolysis was recorded at 486 nm for 20 min (SpectraMAX Plus, Molecular Devices, USA). The measured enzyme activities were quantified based on a percentage of the initial velocity ratio: [$v_i/v_0 \times 100$], where v_i and v_0 are the initial velocities in the presence and absence of halisulfates, respectively. To determine the K_i value and the inhibition mechanism of halisulfate 5 against AmpC BER,

two sets of experiments were performed. The Lineweaver-Burk plots were generated by plotting inverted initial velocities against inversed substrate concentrations (10, 30, 50, 70, and 90 μM) at different concentrations of halisulfate 5 (0, 4, 10, and 20 μM). To get the K_i value, the plots were fitted to the competitive-inhibition equation in the Origin software (OriginLab, USA),

$$v_0 = \frac{v_{max}[S]}{K_m\left(1+\frac{[I]}{K_i}\right)+[S]}$$

where v_{max} is the maximum velocity, [S] represents the nitrocefin concentration, and [I] represents the concentration of halisulfate 5.

2.5. Computational molecular docking

Halisulfates were docked into the active site of the AmpC BER structure by using AutoDock Vina [21]. To prepare the protein for docking, water and sulfate molecules were removed and polar hydrogen atoms were added to the structure of AmpC BER. The three-dimensional structures of halisulfates were generated and optimized with the Builder toolbox in PyMOL (The PyMOL Molecular Graphics System, Version 2.3.2 Schrödinger, LLC).

3. Results and discussion

3.1. Structural feature of the wild-type AmpC BER

There are two AmpC BER molecules (molecules A and B) in the asymmetric unit. They adopt a virtually identical modular structure consisting of a small helical domain (residues 81–167) and a large α/β domain (residues 5–80 and 168–363). The two molecules are superposed with r.m.s. deviation of 0.219 Å for all C^{α} atoms. The active site is situated at the domain interface with the Ω loop and the R2 loop at the opposite boundaries (Fig. 1A). It is divided into the upper R1 site and the lower R2 site with the nucleophilic Ser64 at the border between them (Fig. 1A). The R1 and R2 sites accommodate the R1 and R2 side chains of β-lactam antibiotics, respectively, in the complex structures between class C enzymes and substrates [22–27]. Despite the overall resemblance, the local structure of the *H*10 helix region in the R2 loop, which harbors a two-amino-acid insertion and defines the boundary of the R2 site, is remarkably different in the two AmpC BER molecules. In molecule A, the entire R2 loop is highly ordered as indicated by clear electron density whereas the *H*10 helix region of the R2 loop (residues 284–295) is disordered in molecule B (Fig. 1B). Such a structural difference that is attributable to different packing environments shows the flexible nature of the *H*10 helix region.

3.2. Structural basis for the extended-spectrum activity of AmpC BER

To gain insights into the ES activity of AmpC BER, the structure of AmpC BER (molecule A) is superposed onto that of AmpC EC2 [11]; the r.m.s. deviation for all corresponding C^{α} atoms is 0.261 Å. This comparison uncovers the structural alteration of the R2 loop induced by the insertion mutation in AmpC BER (Fig. 2). Two alanines are inserted between Leu293 and Ala294; as a result, Leu293-Ala294-Ala295-His296 in AmpC EC2 is changed to Leu293-Ala294-Ala295-Ala296-Ala297-His298 in AmpC BER. Concurrently, residues 289–294 in AmpC EC2 and corresponding residues 289–296 in AmpC BER have different organizations of structural elements (Fig. 2). In AmpC EC2, residues 289–293 adopt the helical structure (*H*10 helix) and Ala294 is a one-residue random coil. In contrast, residues 289–292 adopt a random-coil conformation and residues 293–296 form a 3_{10} helix in AmpC BER. Overall, the unfolding of the helical structure in residues 289–293 is accompanied by the coil-to-helix transition of residues 293–296 in AmpC BER.

In AmpC EC2, the *H*10 helix restricts the size of the R2 site due to its location at the boundary (Fig. 2A). Therefore, the transition of residues 289–293 from the thick helical conformation into a thin random-coil has an effect to widen the R2 site in AmpC BER. The shortest distance between the nucleophilic Ser64 and the *H*10 helix is ~ 12.4 Å when measured with the C^{α} atoms of Ser64 and Ala292. It should be noted that the distance between the same atoms is ~ 21.4 Å in AmpC BER, which indicates the ~ 9.0 Å shift of the active site boundary (Fig. 2A). The wider active site is a general feature of ES class C β-lactamases with insertion or deletion mutations at the boundary region. For example, a three-residue insertion in the Ω loop of GC1 and a three-residue deletion in the R2 loop of CMY-10 change the conformation of respective loops at the boundaries to enlarge the active site [10,28].

Class C β-lactamases hydrolyze β-lactam antibiotics through a two-step reaction after forming the non-covalent enzyme-substrate complex [29]. In the first acylation reaction, the attack of the nucleophilic Ser64 on the carbonyl carbon of the lactam ring forms the acyl-enzyme intermediate in which the side-chain hydroxyl oxygen of Ser64 is covalently linked to the carbonyl carbon and the C-N bond in the ring is broken. In the second deacylation reaction, the same carbonyl carbon is attacked by a water molecule to release ring-opened antibiotics and to return Ser64 to its original state. The deacylation reaction is the rate-determining step in the hydrolysis of β-lactam antibiotics [25,30,31]. Therefore, the pose of β-lactam antibiotics in the acyl-enzyme intermediate is critical for the deacylation reaction. Bulky carbapenems and third/fourth-generation cephalosporins bound in the narrow active site adopt catalytically-incompetent poses that are defective in the stabilization of the high-energy tetrahedral deacylation transition state, displace the deacylation water, or block the trajectory of the deacylation water [10,32–34]. However, they can have deacylation-competent poses in the enlarged active site of ES enzymes [28,34]. In this perspective, the high k_{cat} values of AmpC BER towards bulky β-lactam antibiotics are likely to be associated with its widened active site, since the k_{cat} value depends on the rate-determining deacylation step. Furthermore, the low K_m values of AmpC BER towards those substrates appear to be related to the flexible nature of the *H*10 helix region that has an advantage in making favorable contacts with a broad range of β-lactam antibiotics with different R2 side chains.

3.3. Structure-guided search for novel inhibitor scaffolds

Another interesting observation in the crystal structure of AmpC BER is two tightly-bound sulfates in the active site; the source of sulfates seems to be the crystallization solution. From the initial stage of the refinement, two strong difference Fourier electron densities of sulfates were observed in the active site (Fig. 3). The first sulfate (Sul-I) is located near the nucleophilic Ser64 and its three oxygen atoms make multiple polar contacts with active site residues. O2 interacts with the side-chain hydroxyl group of Tyr150 and the side-chain amino group of Lys317. The distance between O4 and the hydroxyl group of Ser64 is 3.1 Å, indicating a hydrogen bonding interaction. O3 is connected to Asn345 and Asn348 through a water-mediated hydrogen-bonding network. The second sulfate (Sul-II) is located between the Ω-loop and the β8 strand in the R1 site. Although only two oxygen atoms of Sul-II are involved in interactions with the active site residues, it is notable that Sul-II interacts with the backbone –NH groups of Ser212 in the Ω-loop and Gly322 in the β8-β9 loop.

Recently, our group discovered that nucleotides including acAMP, IMP, GMP, and NADPH are effective in inhibiting AmpC BER and CMY-10 [12,26,27,35]. According to the crystal structures

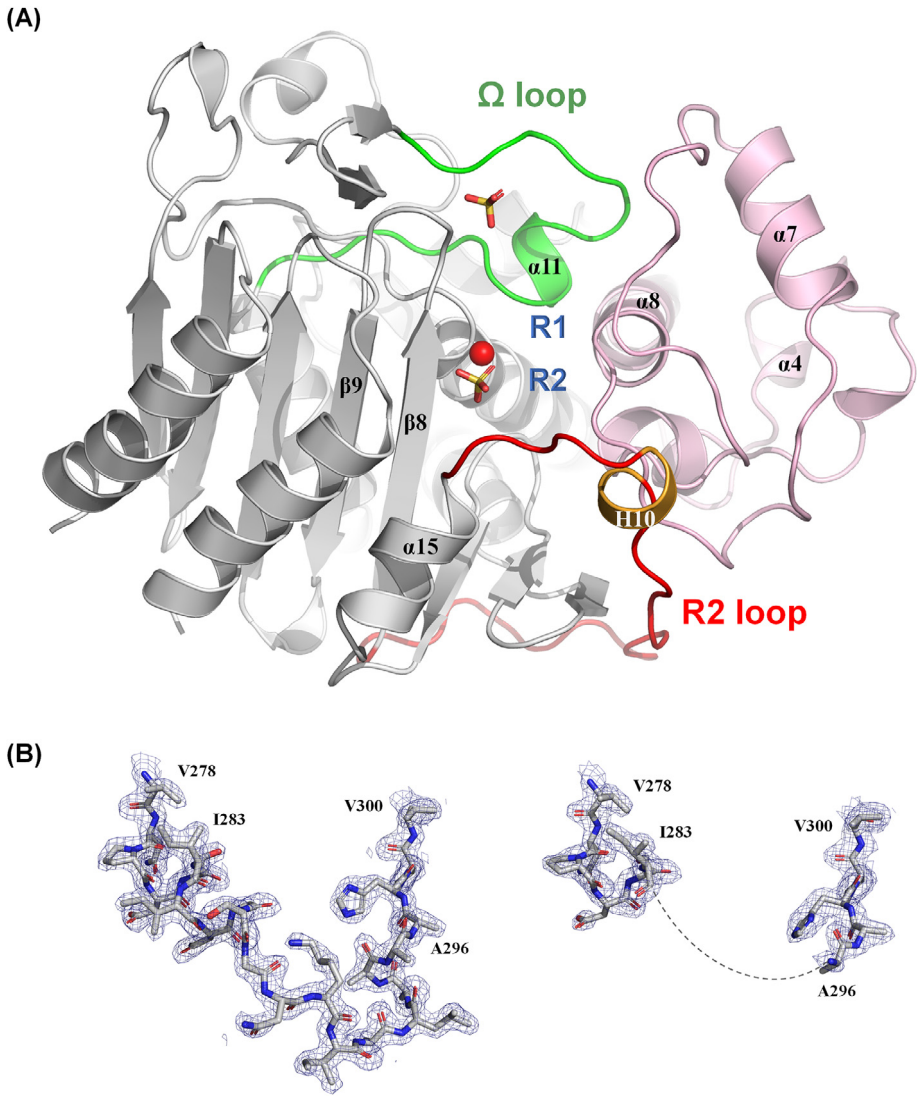

Fig. 1. Overall structure and the conformation of the *H*10 helix region. (A) A cartoon diagram is shown with some secondary structures labeled. The α/β domain, helical domain, Ω loop, R2 loop, and *H*10 helix are colored gray, pink, green, red, and orange, respectively, in all figures. A red sphere represents Ser64 and two sulfates (Sul-I and Sul-II) are shown as sticks. R1 and R2 stand for R1 and R2 subsites, respectively. (B) The final maximum-likelihood weighted $2F_o$-F_c electron density map of residues 278–300 contoured at 1σ (left: molecule A, right: molecule B). The dotted line indicates the disordered part in molecule B. (For interpretation of the references to colour in this figure legend, the reader is referred to the web version of this article.)

of the adenylylated AmpC BER and nucleotide-bound CMY-10 [12,26], the three structural components of nucleotides (the phosphate group, the ribose ring, and the base ring) nicely fit into the active site with geometric and electrostatic complementarities. These discoveries, together with the presence of sulfate-binding subsites in the active site of AmpC BER, prompted us to search for ring-structured compounds with phosphate or sulfate groups to examine whether they would have an inhibitory effect on AmpC BER.

Halisulfates were isolated from *Coscinoderma* sp. collected at Chuuk, Micronesia [20]. Their structures satisfy our selection criteria in that they have rings and a sulfate group (Fig. 4). Halisulfates 1, 3, and 5, which are used in this study, are featured by a sulfate group, a monocyclic ring, and a bicyclic ring. Halisulfates 3 and 5 have the virtually identical aliphatic carbon chain except for the stereochemistry at C-13 that is not defined in halisulfate 5. The only structural difference in the two halisulfates resides in the bicyclic ring (Fig. 4). On the other hand, their carbon chains are remarkably different from that of halisulfate 1 (Fig. 4). Halisulfates 3 and 5 have a fully saturated chain of six carbon atoms whereas halisulfate 1 has a carbon chain of nine atoms with a double bond and two methyl substituents. In addition to the distinct carbon chains, a methyl sulfate group at C-13 and a furan ring in halisulfates 3 and 5 contrast with a sulfate group at C-12 and a hydroquinone ring in halisulfate 1.

3.4. Molecular docking models of the AmpC BER/halisulfates complexes

To examine whether the halisulfate scaffold would fit into the active site of AmpC BER, we docked the three halisulfates into the active site of AmpC BER (Fig. 5A). In the docked complexes, the sulfate groups of halisulfates nestle in the positively-charged surface region, interacting with the side-chain amino group of Lys317, the side-chain amide group of Asn348, the side-chain guanidium group of Arg351, and the backbone –NH groups of Gly319 and Ala320 (Fig. 5B). This binding mode is reminiscent of the Sul-I binding in AmpC BER and the phosphate-binding in CMY-10 complexed with nucleotides (Fig. S3). Hydrophobic bicyclic rings of the three halisulfates are commonly placed in the space between the small helical domain and the R2 loop (Fig. 5E). The hydrocarbon side chains of Leu119, Leu149, and Tyr150 in the helical domain,

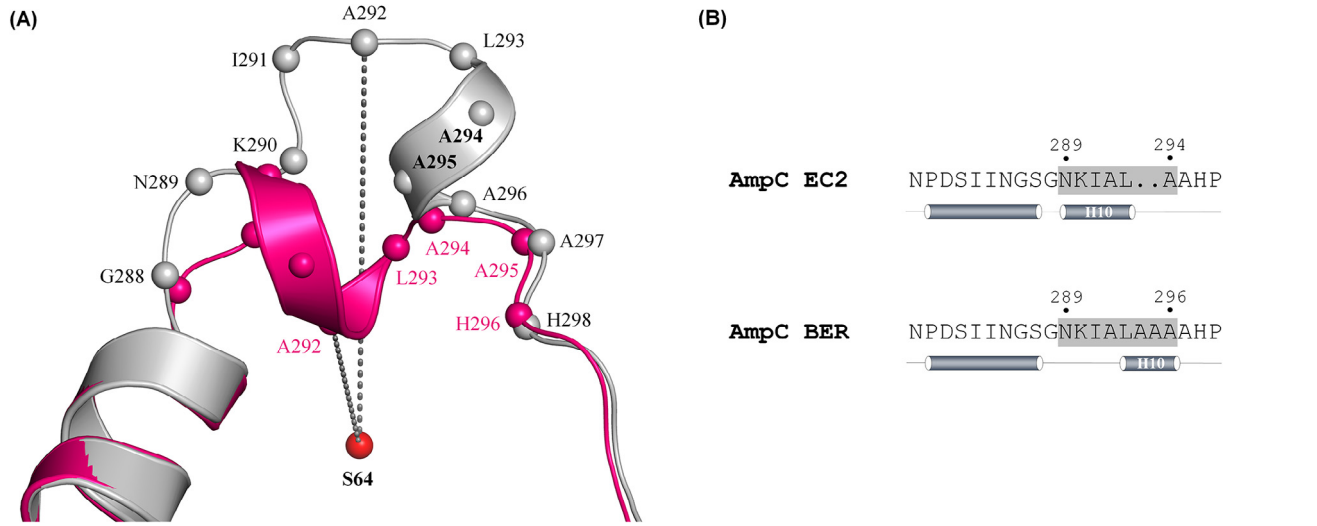

Fig. 2. Structural comparison of the *H*10 helix region. (A) Structures of AmpC BER (gray) and AmpC EC2 (hot pink) are superimposed for this figure. For clarity, only the *H*10 helix regions are shown and C^{α} atoms are presented in spheres. A red sphere represents Ser64 and distances between Ser64 and Ala292 are represented by dotted lines. (B) Structure-based sequence alignment of AmpC BER and AmpC EC2. The *H*10 helix regions are highlighted in gray. (For interpretation of the references to colour in this figure legend, the reader is referred to the web version of this article.)

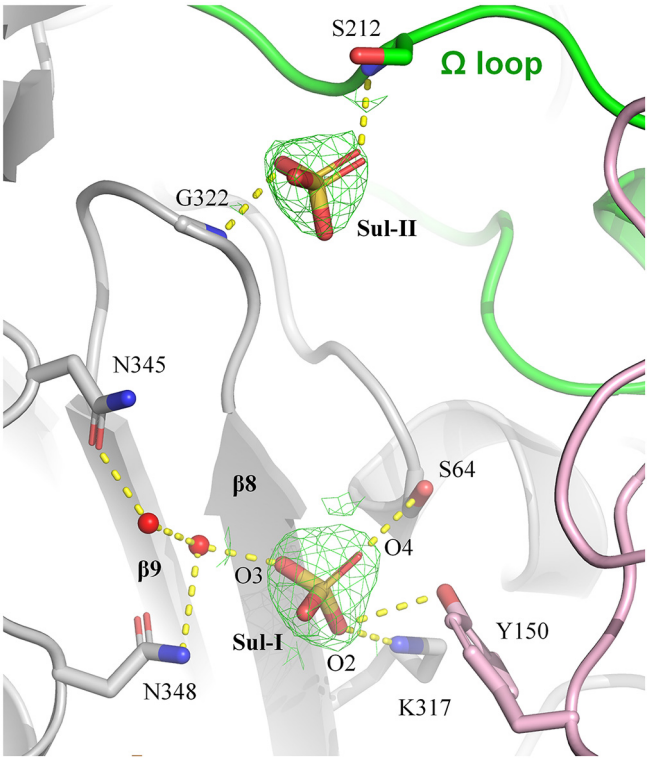

Fig. 3. Binding mode of sulfates. Sulfates and interacting residues are represented as sticks. Water molecules are shown as red spheres. Yellow dotted lines represent polar interactions. The initial maximum-likelihood weighted F_o-F_c electron density maps of sulfates are contoured at 3σ. (For interpretation of the references to colour in this figure legend, the reader is referred to the web version of this article.)

together with the aliphatic part of the Lys290 side chain and the 3_{10} helix in the R2 loop, grip the hydrophobic bulky rings.

A distinctive feature among the three docked structures is the position of the monocyclic ring. The furan rings of halisulfate 3 and 5 are bound to an inner cavity of the R2 site formed by the helix α15, Glu272, His316, and Thr318 (Fig. 5C). Furan rings lean against the C-terminal end of the helix α15 with their oxygen atoms hydrogen-bonded to the imidazole side chain of His316. The negatively-charged carboxylate in the side chain of Glu272 is ~ 3.4 Å away from the furan rings. This unfavorable contact of the non-polar ring with a charged group on one side is likely to facilitate the hydrophobic contact of the ring with the C-terminal end of the helix on the other side. Consequently, the two ring moieties are placed on the same side with reference to the sulfate group with a cis configuration (Fig. 5A). On the other hand, the hydroquinone ring of halisulfate 1 is located in the R1 site; in this trans binding mode, the two ring moieties are located on the opposite sides of the sulfate group (Fig. 5A and D). It appears that the longer halisulfate 1 than halisulfates 3 and 5 is too bulky to adopt a cis configuration in the R2 site. The hydroquinone ring forms a π-π stacking interaction with the aromatic side chain of Tyr221, and the two hydroxyl groups at both ends of the hydroquinone ring are hydrogen-bonded to the side-chain carbonyl group of Gln120 and the backbone –NH group of Gly322 (Fig. 5D). Nevertheless, the trans conformation of halisulfate 1 appears be unfavorable because the hydrophobic aliphatic chain of halisulfate 1 is exposed to the solvent and sandwiched by not hydrophobic residues but polar residues including Ser64, Gln120, Asn152, and Thr321 (Fig. 5D). As described below, halisulfates 3 and 5 with the cis binding mode exhibit higher inhibition activities toward AmpC BER than halisulfate 1 with the unfavorable trans binding mode. The distinct inhibition activities of the two binding modes are not reflected in the similar docking scores of halisulfates. It is notable that the mismatch between docking scores and experimental activities is not a rare case in molecular docking studies [36,37].

The presence of well-defined structural water molecules in the active site is not necessarily helpful to predict the pose of a ligand in molecular docking studies [38]. As shown in Fig. 3, Sul-I is linked to a water-mediated hydrogen bonding network. However, the incorporation of the Sul-I interacting water molecules has little effect on the pose of halisulfates except for the slight shift of the sulfate group for the formation of a hydrogen bond with a water molecule. Therefore, molecular docking was performed in the absence of water molecules in this study.

3.5. Inhibition activities of halisulfates against the ES class C β-lactamase AmpC BER

The successful docking of halisulfates in the active site drove us to examine the inhibitory effects of the three halisulfates on AmpC

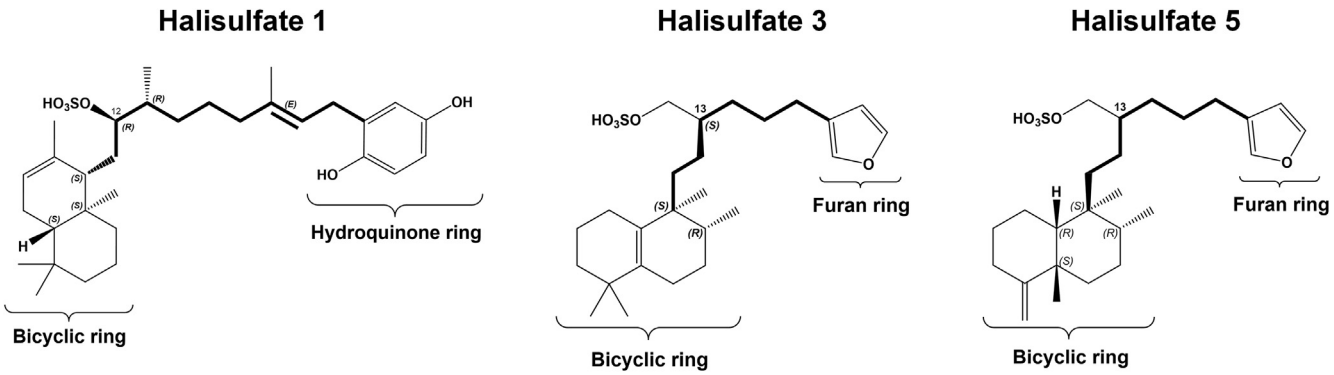

Fig. 4. Chemical structures of halisulfate 1, halisulfate 3, and halisulfate 5. Aliphatic carbon chains are highlighted by bold lines.

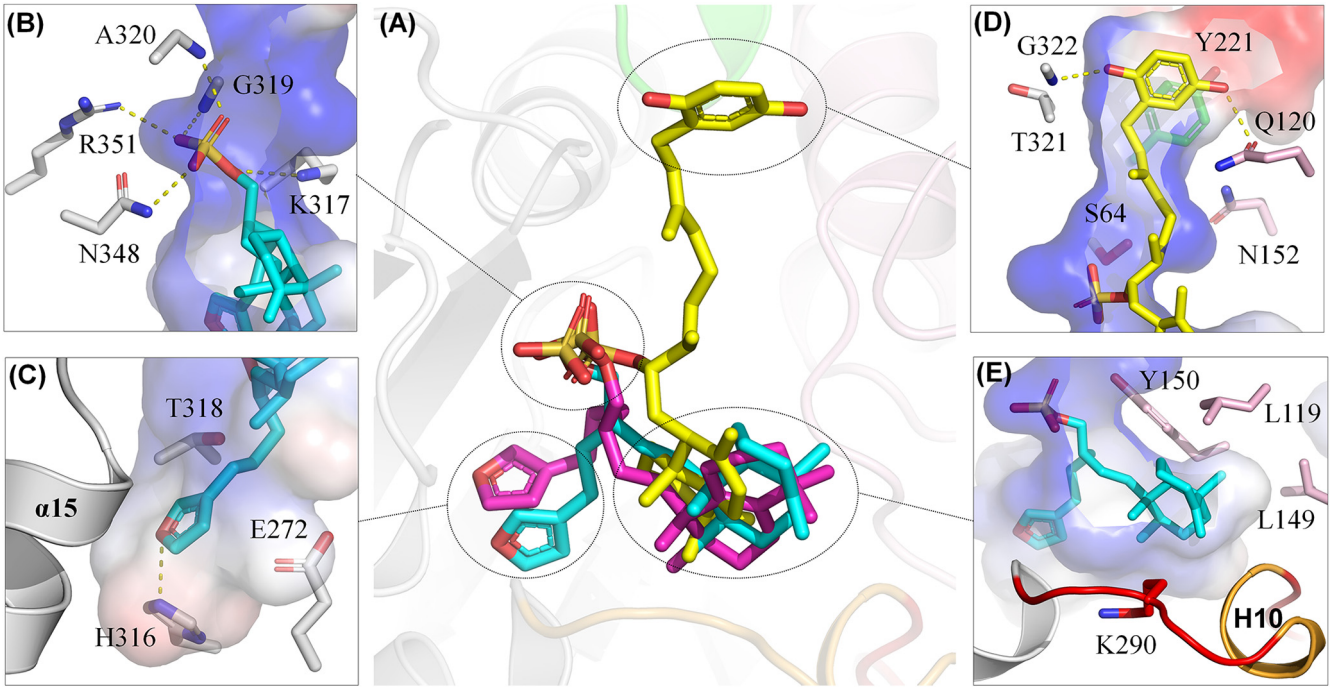

Fig. 5. Binding modes of halisulfates. (A) Halisulfate 1, halisulfate 3, and halisulfate 5 in the active site of AmpC BER are colored in yellow, magenta, and cyan, respectively. The sulfate groups, monocyclic rings, and bicyclic rings are highlighted by dotted circles. Detailed interaction modes of a sulfate group, a furan ring, a hydroquinone ring, a bicyclic ring of halisulfates are presented in (B), (C), (D), and (E), respectively. For clarity, only halisulfates 1 and 5 are shown in (B), (C), (D), and (E). Cavities and pockets of the active site are represented by electrostatic potential surfaces. Blue, red, and white colors indicate positively-charged, negatively-charged, and hydrophobic surfaces, respectively. Yellow dotted lines indicate polar interactions. (For interpretation of the references to colour in this figure legend, the reader is referred to the web version of this article.)

BER with nitrocefin as a reporter substrate. The clinically-used avibactam was employed as a positive control to evaluate the inhibition efficiencies of halisulfates (Fig. 6A). Halisulfates 3 and 5 gave rise to > 97% reduction in the nitrocefin-hydrolyzing activities of AmpC BER, whereas halisulfate 1 exhibited little inhibition activity. In a structural aspect, halisulfates 3 and 5 are very similar to each other but they are different from halisulfate 1 as described above (Fig. 4), which indicates that the structural resemblance and difference among the three halisulfates are related to their distinct inhibition activities.

At 200 μM, halisulfates 3 and 5 seemed to be as effective as avibactam in inhibiting the nitrocefin-hydrolyzing activity of AmpC BER (Fig. 6A). To determine the inhibition mechanism and the equilibrium constant for inhibitor binding to the enzyme (K_i), halisulfate 5 was selected as a model compound for steady-state kinetics due to its somewhat higher inhibition activity compared to halisulfate 3 (Fig. 6A). In the presence of halisulfate 5, K_m and k_{cat} of AmpC BER towards nitrocefin were increased and kept constant, respectively, which indicates that halisulfate 5 acts as a competitive inhibitor that occupies the active site to prevent the binding of nitrocefin (Fig. 6B). The K_i value of halisulfate 5 toward AmpC BER was calculated to be 5.87 μM. It is also notable that the inhibition of AmpC BER by halisulfate 5 was not time-dependent.

3.6. Inhibition activities of halisulfates on other types of β-lactamases

Encouraged by the efficient inhibitory activities of halisulfates 3 and 5 against AmpC BER, we tested whether halisulfates also inhibit other classes of serine β-lactamases (Class A: KPC-2, Class C: CMY-10, and Class D: OXA-10). Among the tested enzymes, the nitrocefin-hydrolyzing activity of CMY-10 was most noticeably affected by halisulfates (Fig. 7). CMY-10 is a different type ES class C enzyme with a 43.3% sequence identity to AmpC BER. Consistent with the inhibition pattern for AmpC BER, halisulfates 3 and 5 were

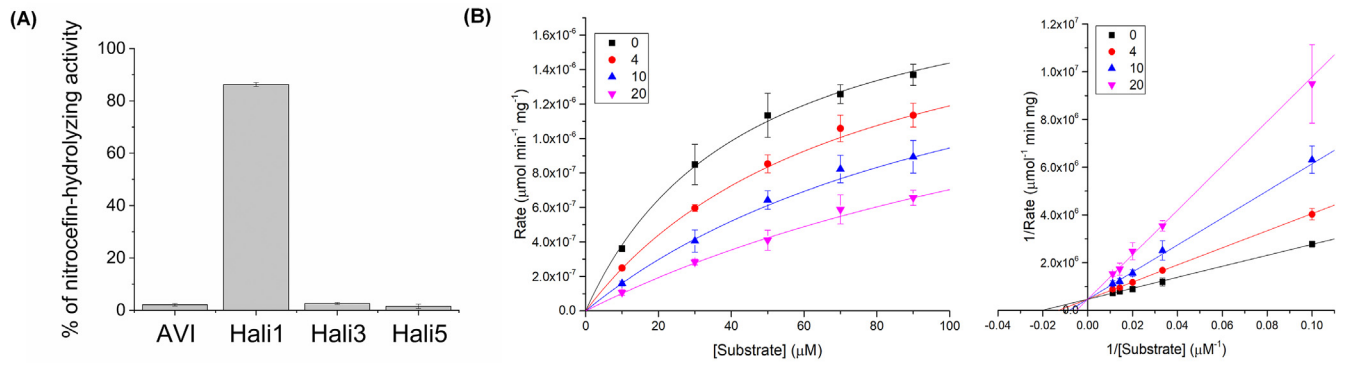

Fig. 6. Inhibition activities of halisulfates against AmpC BER. (A) Percent changes in the nitrocefin-hydrolyzing activities of AmpC BER. AVI, Hali 1, Hali 3, and Hali 5 are abbreviations for avibactam, halisulfate 1, halisulfate 3, and halisulfate 5, respectively. (B) Michaelis-Menten (left) and Lineweaver-Burk (right) plots.

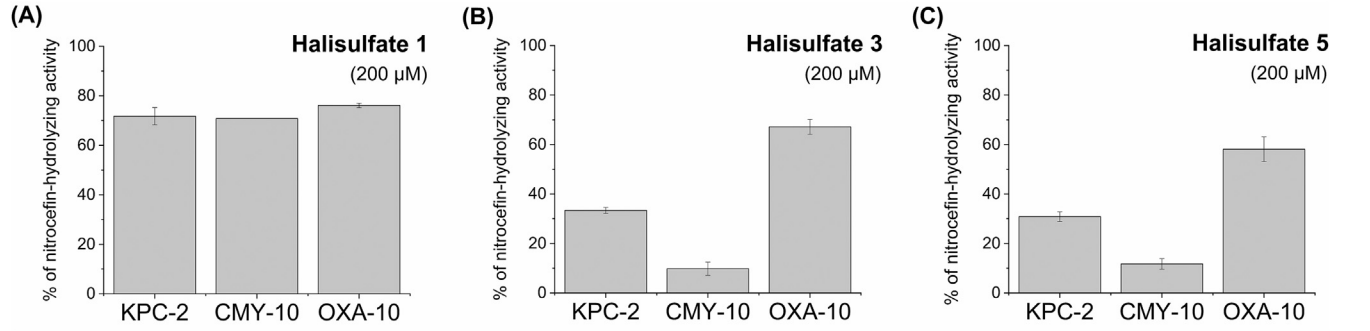

Fig. 7. Inhibition activities of halisulfates against serine β-lactamases. Percent changes in nitrocefin-hydrolyzing activities of enzymes in the presence of 200 μM (A) halisulfate 1, (B) halisulfate 3, and (C) halisulfate 5.

better at inhibiting CMY-10 than halisulfate 1 (Fig. 7); the activity of CMY-10 was reduced up to ~ 90% by halisulfates 3 and 5, which suggest that they are efficient in inhibiting diverse class C enzymes. In addition, it was confirmed that halisulfates 3 and 5 displayed moderate and weak inhibition activities against KPC-2 and OXA-10, respectively (Fig. 7B and C). Further studies were conducted on metallo-β-lactamase, NDM-1 (Fig. 8). Although a higher concentration of halisulfates (1 mM) was used compared to other tests, the inhibition activities of halisulfates 3 and 5 were identified by reducing the enzyme activities up to 30 ~ 40%. Since so far there is no clinically-introduced inhibitor for class B β-lactamases, it is worth noting that halisulfates 3 and 5 inhibit class B enzymes.

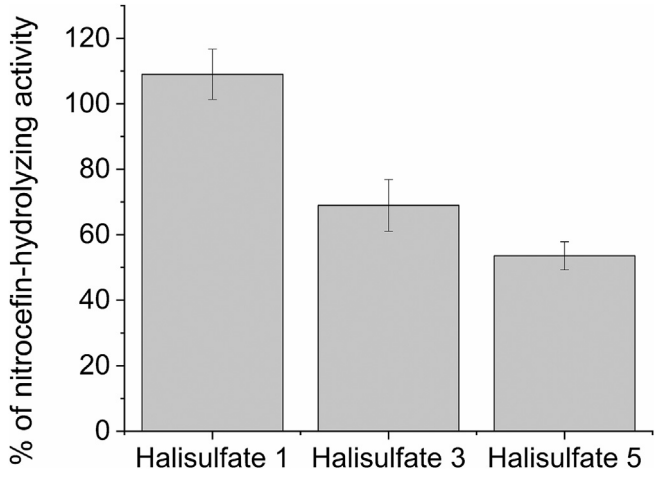

Fig. 8. Percent changes in the nitrocefin-hydrolyzing activity of metallo-β-lactamase NDM-1 against 1 mM halisulfates.

4. Conclusions

Consequently, we discovered that halisulfates 3 and 5 reduced the nitrocefin-hydrolyzing activities of KPC-2, NDM-1, AmpC BER, CMY-10, and OXA-10. Especially, halisulfate 5 inhibits ES class C β-lactamase AmpC BER with the K_i value of 5.87 μM in a competitive manner. The broad inhibition spectrum of halisulfates indicates that their structural scaffold could be used to develop novel inhibitors that can escape bacterial resistance mechanisms mediated by β-lactamases. One idea for structural modification of halisulfates is as follows. Halisulfates have hydrophobic properties derived from carbon rings and chains in their structures, which limits not only their solubility but also their inhibition activities against β-lactamases considering the presence of many polar residues in the active site. Therefore, introducing additional hydrophilic groups in the hydrophobic portions of halisulfates would be necessary to develop innovative inhibitors targeting all classes of β-lactamases.

5. Accession number

The coordinates and structure factors of AmpC BER have been deposited in the Protein Data Bank with the accession code 7CIN.

CRediT authorship contribution statement

Bo-Gyeong Jeong: Methodology, Formal analysis, Writing - original draft. **Jung-Hyun Na:** Methodology. **Da-Woon Bae:**

Methodology, Writing - original draft. **Soo-Bong Park:** Methodology. **Hyi-Seung Lee:** Methodology, Resources, Writing - original draft, Funding acquisition. **Sun-Shin Cha:** Supervision, Conceptualization, Investigation, Writing - original draft, Funding acquisition.

Declaration of Competing Interest

The authors declare that they have no known competing financial interests or personal relationships that could have appeared to influence the work reported in this paper.

Acknowledgments

We thank the beamline staff at Pohang Light Source and Photon Factory. We are grateful to the Department of Marine Resources, State of Chuuk, Federated States of Micronesia, for supporting marine organism research. This study was supported by the Korea Polar Research Institute (PM20030); the Ministry of Oceans and Fisheries (the project entitled "Development of Biomedical materials based on marine proteins", the Collaborative Genome Program of KIMST (No. 20180430), and PM62060); and the National Research Foundation of Korea (NRF-2015M1A5A1037480 and NRF-2020R1F1A1075469).

Appendix A. Supplementary data

Supplementary data to this article can be found online at https://doi.org/10.1016/j.csbj.2020.12.015.

References

[1] Munita JM, Arias CA. Mechanisms of Antibiotic Resistance. Microbiol Spectr. 2016;4.
[2] Tooke CL, Hinchliffe P, Bragginton EC, Colenso CK, Hirvonen VH, Takebayashi Y, et al. β-Lactamases and β-lactamase inhibitors in the 21st century. J Mol Biol 2019;431:3472–500.
[3] Drawz SM, Bonomo RA. Three decades of β-lactamase inhibitors. Clin Microbiol Rev. 2010;23:160–201.
[4] Ehmann DE, Jahić H, Ross PL, Gu R-F, Hu J, Durand-Réville TF, et al. Kinetics of avibactam inhibition against class A, C, and D β-lactamases. J Biol Chem 2013;288:27960–71.
[5] Lomovskaya O, Sun D, Rubio-Aparicio D, Nelson K, Tsivkovski R, Griffith DC, et al. Vaborbactam: spectrum of beta-lactamase inhibition and impact of resistance mechanisms on activity in *Enterobacteriaceae*. Antimicrob Agents Chemother 2017;61:e01443–e1517.
[6] Shields RK, Chen L, Cheng S, Chavda KD, Press EG, Snyder A, et al. Emergence of ceftazidime-avibactam resistance due to plasmid-borne bla_{KPC-3} mutations during treatment of carbapenem-resistant *Klebsiella pneumoniae* infections. Antimicrob Agents Chemother 2017;61:e02097–e2116.
[7] Mammeri H, Poirel L, Nordmann P. Extension of the hydrolysis spectrum of AmpC β-lactamase of *Escherichia coli* due to amino acid insertion in the H-10 helix. J Antimicrob Chemother 2007;60:490–4.
[8] Nukaga M, Haruta S, Tanimoto K, Kogure K, Taniguchi K, Tamaki M, et al. Molecular evolution of a class C β-lactamase extending its substrate specificity. J Biol Chem 1995;270:5729–35.
[9] Zhang Z, Yu Y, Musser JM, Palzkill T. Amino acid sequence determinants of extended spectrum cephalosporin hydrolysis by the class C P99 β-lactamase. J Biol Chem 2001;276:46568–74.
[10] Kim JY, Jung HI, An YJ, Lee JH, Kim SJ, Jeong SH, et al. Structural basis for the extended substrate spectrum of CMY-10, a plasmid-encoded class C β-lactamase. Mol Microbiol 2006;60:907–16.
[11] Na J-H, Cha S-S. Structural basis for the extended substrate spectrum of AmpC BER and structure-guided discovery of the inhibition activity of citrate against the class C β-lactamases AmpC BER and CMY-10. Acta Crystallographica Section D: Structural Biology. 2016;72:976–85.
[12] Kim M-K, An YJ, Na J-H, Seol J-H, Ryu JY, Lee J-W, et al. Structural and mechanistic insights into the inhibition of class C β-lactamases through the adenylylation of the nucleophilic serine. J Antimicrob Chemother 2017;72:735–43.
[13] An YJ, Ahn B-E, Roe J-H, Cha S-S. Crystallization and preliminary X-ray crystallographic analyses of Nur, a nickel-responsive transcription regulator from *Streptomyces coelicolor*. Acta Crystallogr, Sect F: Struct Biol Cryst Commun 2008;64:130–2.
[14] An Y, Kim M, Song J, Kang M, Lee Y, Cha S. Vapor batch crystallization and preliminary X-ray crystallographic analysis of a cold-active endo-β-1, 4-glucanase that was produced through the cold temperature protein expression. Biodesign. 2015;3:138–42.
[15] Otwinowski Z, Minor W. HKL Denzo and Scalepack. Methods Enzymol 1997;276:307–26.
[16] Vagin A, Teplyakov A. Molecular replacement with MOLREP. Acta Crystallogr D Biol Crystallogr 2010;66:22–5.
[17] Emsley P, Cowtan K. Coot: model-building tools for molecular graphics. Acta Crystallogr D Biol Crystallogr 2004;60:2126–32.
[18] Liebschner D, Afonine PV, Baker ML, Bunkóczi G, Chen VB, Croll TI, et al. Macromolecular structure determination using X-rays, neutrons and electrons: recent developments in Phenix. Acta Crystallographica Section D: Structural Biology. 2019;75:861–77.
[19] Lee H-S, Lee T-H, Yang SH, Shin HJ, Shin J, Oh K-B. Sesterterpene sulfates as isocitrate lyase inhibitors from tropical sponge *Hippospongia sp*. Bioorg Med Chem Lett 2007;17:2483–6.
[20] Lee D, Shin J, Yoon K-M, Kim T-I, Lee S-H, Lee H-S, et al. Inhibition of *Candida albicans* isocitrate lyase activity by sesterterpene sulfates from the tropical sponge *Dysidea* sp. Bioorg Med Chem Lett 2008;18:5377–80.
[21] Trott O, Olson AJ. AutoDock Vina: improving the speed and accuracy of docking with a new scoring function, efficient optimization, and multithreading. J Comput Chem 2010;31:455–61.
[22] Usher KC, Blaszczak LC, Weston GS, Shoichet BK, Remington SJ. Three-dimensional structure of AmpC β-lactamase from *Escherichia coli* bound to a transition-state analogue: possible implications for the oxyanion hypothesis and for inhibitor design. Biochemistry 1998;37:16082–92.
[23] Beadle BM, Shoichet BK. Structural basis for imipenem inhibition of class C β-lactamases. Antimicrob Agents Chemother 2002;46:3978–80.
[24] Wouters J, Fonze E, Vermeire M, Frère J-M, Charlier P. Crystal structure of *Enterobacter cloacae* 908R class C β-lactamase bound to iodo-acetamido-phenyl boronic acid, a transition-state analogue. Cellular and Molecular Life Sciences CMLS. 2003;60:1764–73.
[25] Nukaga M, Kumar S, Nukaga K, Pratt RF, Knox JR. Hydrolysis of third-generation cephalosporins by class C β-lactamases structures of a transition state analog of cefotaxime in wild-type and extended spectrum enzymes. J Biol Chem 2004;279:9344–52.
[26] Na J-H, An YJ, Cha S-S. GMP and IMP are competitive inhibitors of CMY-10, an extended-spectrum class C β-lactamase. Antimicrob Agents Chemother 2017;61.
[27] Bae D-W, Jung Y-E, An YJ, Na J-H, Cha S-S. Structural insights into catalytic relevances of substrate poses in ACC-1. Antimicrob Agents Chemother 2019;63:e01411–e1419.
[28] Crichlow GV, Kuzin AP, Nukaga M, Mayama K, Sawai T, Knox JR. Structure of the extended-spectrum class C β-lactamase of *Enterobacter cloacae* GC1, a natural mutant with a tandem tripeptide insertion. Biochemistry 1999;38:10256–61.
[29] Galleni M, Frère J-M. A survey of the kinetic parameters of class C β-lactamases. Penicillins. Biochemical Journal. 1988;255:119–22.
[30] Mazzella LJ, Pratt R. Effect of the 3′-leaving group on turnover of cephem antibiotics by a class C β-lactamase. Biochem J 1989;259:255–60.
[31] Nukaga M, Taniguchi K, Washio Y, Sawai T. Effect of an amino acid insertion into the omega loop region of a class C β-lactamase on its substrate specificity. Biochemistry 1998;37:10461–8.
[32] Oefner C, d'Arcy A, Daly J, Gubernator K, Charnas R, Heinze I, et al. Refined crystal structure of β-lactamase from *Citrobacter freundii* indicates a mechanism for β-lactam hydrolysis. Nature 1990;343:284–8.
[33] Heinze-Krauss I, Angehrn P, Charnas RL, Gubernator K, Gutknecht E-M, Hubschwerlen C, et al. Structure-based design of β-lactamase inhibitors. 1. Synthesis and evaluation of bridged monobactams. J Med Chem 1998;41:3961–71.
[34] Powers RA, Caselli E, Focia PJ, Prati F, Shoichet BK. Structures of ceftazidime and its transition-state analogue in complex with AmpC β-lactamase: implications for resistance mutations and inhibitor design. Biochemistry 2001;40:9207–14.
[35] Na J-H, Lee TH, Park S-B, Kim M-K, Jeong B-G, Chung KM, et al. *In vitro* and *in vivo* inhibitory activity of NADPH against the AmpC BER class C β-lactamase. Front Cell Infect Microbiol 2018;8:441.
[36] Ramírez D, Caballero J. Is it reliable to use common molecular docking methods for comparing the binding affinities of enantiomer pairs for their protein target?. Int J Mol Sci 2016;17:525.
[37] Prieto-Martínez FD, Arciniega M, Medina-Franco JL. Molecular docking: current advances and challenges. TIP Revista Especializada en Ciencias Químico-Biológicas. 2019;21:65–87.
[38] Wong SE, Lightstone FC. Accounting for water molecules in drug design. Expert Opin Drug Discov 2011;6:65–74.